Cell Affinity Separations Using Magnetically Stabilized Fluidized Beds

Erythrocyte Subpopulation Fractionation Utilizing a Lectin-Magnetite Support

David D. Putnam, Vijay Namasivayam, Mark A. Burns

Department of Chemical Engineering, University of Michigan, Ann Arbor, Michigan 48109; telephone: 734-764-4315; fax: 734-763-0459; e-mail: maburns@umich.edu

Received 12 October 2001; accepted 31 July 2002

DOI 10.1002/bit.10511

Abstract: A magnetically stabilized fluidized bed is used to separate erythrocyte subpopulations. Binding specificity was obtained by immobilizing the lectin *Helix pomatia* Agglutinin (HpA) or *Griffonia simplicifolia* I (GSI) onto a magnetite-containing support. Separation of type A and type O erythrocytes with the lectin HpA was particularly effective, leading to a 94% purity of retained type A erythrocytes. A 3.1 ± 0.6 log removal of type A erythrocytes was also accomplished leading to a 99.7% ± 0.4% purity and 95% ± 7% yield of type O erythrocytes in the collected effluent. Elution of the purified cells was accomplished using fluidization in the presence of a sugar competing for the lectin–erythrocyte binding site. A mathematical model based on the depth filtration model of Putnam and Burns (Chem Eng Sci 1997;52(1): 93–105) was extended to include multicomponent cell adhesion. This filtration model is the first to take into account the finite binding capacity of the chromatographic support and is used to characterize the cell binding behavior and to determine optimal parameters and conditions that lead to high capacities and selectivities. Model parameter values and observations from in situ adsorption studies suggest that the non-spherical shape of the magnetite-based support allows for a more efficient utilization of the support surface area than the spherical shape. Using a 1.5-cm diameter laboratory column and realistic parameter values, the processing rates of the system are predicted to be at least an order of magnitude greater than the 10^8/h cells that can typically be processed in packed bed cell affinity chromatography (CAC) systems. *Biotechnol Bioeng* **81:** 650–665, 2003.

Keywords: cell affinity; lectins; erythrocytes; modeling; adsorption; adhesion

INTRODUCTION

The ability to separate and analyze cell populations is required in a number of biotechnology and biomedical applications. For example, the characterization of the various T cell subpopulations and their control of the immune system has led to the development of classes of drugs known as interleukins and interferons that are used to treat a variety of immunotherapy diseases (Fitzgibbons, 1996). Hematopoietic stem cells isolated from bone marrow cells have been targeted for a number of clinical transplantation applications, including tumor cell purging, T cell depletion, stem cell expansion, and gene therapy (Collins, 1994).

Of the various devices available for cell separations, by far the most selective cell separation system is the fluorescent activated cell sorter (FACS) that individually sorts cells based on their light scattering and emission characteristics. Körbling and co-workers (1994) reported the ability to separate one $CD34^+$, DR^- hemotopoietic progenitor cell out of 8000 nucleated cells by staining the $CD34^+$, DR^- cells with a fluorescent conjugated antibody. Despite their incredible selectivity, the limited throughput (10^7/h) and the high expense of these systems have somewhat restricted their application. More recently, a novel cell separation technique mediated by differential rolling adhesion was reported (Greenberg, 2001). This technique exploits differences in average rolling velocities of various cell populations on L-selectin chimeric substrates under well-defined flows.

Due to their low cost and simple operation, cell affinity chromatography (CAC) systems are increasingly being used for the isolation of a variety of immune cell types (Putnam et al., 1999). CAC relies on the interaction of cell surface-bound molecules and their complementary ligands (monoclonal antibodies, lectins). If a ligand is covalently bound to a chromatographic support and is accessible to passing cells, then the cells possessing the appropriate cell surface molecules could be removed from the solution. Yields are typically greater than 50%, and purities can be comparable to fluorescent activated cell sorters (Braun et al., 1982; de Wynter et al., 1991). In two hours, 10^8–10^9 cells can easily be processed, a minimum amount typically necessary for laboratory or clinical use.

Correspondence to: Mark A. Burns

Contract grant sponsors: National Science Foundation; Donors of the Petroleum Research Fund (administered by the American Chemical Society); National Institutes of Health

Contract grant numbers: CTS-9216078; 5-R01-GM08353

Several types of molecules can be used as CAC ligands. For example, lectins, a class of proteins that bind carbohydrates (Sharon, 1983; Sharon and Lis, 1989), are particularly attractive ligands since many cell types differ in their cell surface sugars. Lectins are polyvalent and can form multiple cell–ligand bonds, allowing these proteins to be used to separate cell subpopulations by selective agglutination. In fact, the early success of bone marrow transplantation was facilitated by first removing a large number of T lymphocytes by agglutination with the lectin soybean agglutinin (Reisner et al., 1981). Removal of T cells from the donor marrow is a necessary step to reduce the chance of the patient developing graft-versus-host disease, the major cause of mortality after allogeneic bone marrow transplantation (Kernan, 1994).

In addition to selective agglutination, lectins have also found extensive use in packed bed cell affinity chromatography systems (Putnam et al., 1999; Sharma and Mahendroo, 1980). The advantage of packed bed CAC over agglutination is the increase in throughput of the system. The disadvantage of such devices is that, due to the flow constrictions around the packed particles, the bed can easily clog from specific and/or nonspecific binding.

We have found that a magnetically stabilized fluidized bed (MSFB) allows for higher processing rates and a wider range of operating conditions than conventional packed bed CAC columns. The MSFB is a fluidized bed containing a magnetically susceptible support stabilized in a low-power magnetic field. With the bed fluidized, the pressure drop across the column is independent of the flow rate. Therefore, high flow rates can be used that would otherwise lead to bed compaction and subsequent physical entrapment of cells in packed beds. With fluidization, long bed heights and high liquid velocities can be used, allowing increased processing rates. Continuous operation is also possible due to the fluid-like nature of the bed (Burns and Graves, 1985).

MSFBs have higher efficiencies than packed beds due to their lower surface shear rates. These low shear rates are due primarily to the expanded nature of the packing material. Other expanded bed adsorption systems (Chase, 1994) also have low shear rates but suffer from packing material mixing. This mixing, which is eliminated in magnetically stabilized beds, reduces cell capture by increasing cell desorption and bed instabilities (Riley, 1989; Terranova and Burns, 1991).

In this paper, we use blood type specific lectins (Sharon and Lis, 1989) to purify different mixtures of erythrocyte subpopulations in an MSFB. The affinity support in the MSFB is a non-porous magnetite (Fe_3O_4) with surface-bound lectin. Adapting our recent model for cell removal in packed bed depth filters (Putnam and Burns, 1997), we have quantified the binding behavior of these cell populations and used the model to explore the effect of several experimental and model parameters on the processing capacity and selectivity of the system.

THEORETICAL MODEL

The purpose of the model is to predict the concentration of individual cell populations processed in the bed as a function of time. This information can be used to determine parameter ranges that correspond to maximum target cell binding and selectivity. The model is general enough to describe our MSFB system as well as a packed bed cell affinity chromatography (CAC) systems.

As described earlier (Putnam and Burns, 1997), the model consists of differential mass balances on the bed and fluid phase coupled by an adsorption rate expression. These equations must now be written for each cell population. Dispersive terms in the mass balances are neglected since stabilization eliminates support-particle mixing. Studies using typical experimental conditions have shown that liquid dispersion has a negligible effect on bed performance when the Peclet number is greater than 100 (Putnam and Burns, 1997).

The adsorption rate expression for each cell population couples the two mass balance equations (Putnam and Burns, 1997) and is given by

$$R_{a,i} = \frac{3}{2d}(1-\varepsilon)^{1/3} v_l c_i \eta_i, \tag{1}$$

where c is the concentration in the liquid (number of cells per unit volume of liquid), d is the support diameter, ε is the void fraction, and v_l is the superficial liquid velocity. Given the strong binding on affinity based supports, cell desorption is neglected.

In this expression, η_i is the collection efficiency of the support for cell population i and is defined as the fraction of cells approaching the support that become bound. η_i takes into account the transport and binding of cells to the surface of the support and the decrease in collection efficiency as the capacity of the support is utilized. This behavior is expressed mathematically as

$$\eta_i = \eta_{0,i} P_i \left(1 - \sum_i \psi_i\right)^{\beta_i}, \tag{2}$$

where $\eta_{0,i}$ is, for each population, the fraction of cells whose trajectories lead to contact with the support, P_i is an adhesion efficiency of population i. η_0 is referred to in the depth filtration literature as the initial collection efficiency (Putnam and Burns, 1997).

ψ_i is the fraction of the support area occupied by a given population (assuming monolayer coverage), and β_i is a shadowing rate exponent for that population:

$$\psi_i = \frac{\sigma_i}{\sigma_{m,i}} = \frac{\sigma_i}{(6s(1-\varepsilon)/d\pi a_i^2)} = \frac{\text{Projected surface area of bound cells}}{\text{Area avilable for binding assuming monolayer coverage}}. \tag{3}$$

For spherical supports, the area initially available for collection is one half the total surface area ($s = 0.5$). However,

for binding on irregularly shaped supports, a larger value may need to be used (see Results and Discussion). As discussed by Putnam and Burns (1997), because of its large size, a bound cell can block the binding of suspended cells with the support surface, effectively blocking or shadowing other downstream sites. This leads to a non-linear decrease in adsorption rate as ψi increases ($\beta_i > 1$). a is the cell radius, and σ is the specific deposit (number of cells bound per unit bed volume).

The selectivity of the bed is accounted for in Eq. (2) by an adhesion efficiency, P, for each cell population. The probability of binding is not constant over the support surface because the shear rate (the force per unit area that a cell must counteract to remain bound) is a strong function of position and greatly affects cell binding. Also taken into account is the fact that the probability of contact with a particular position on the support is not constant across the support surface (Jung and Tien, 1993; Mackie et al., 1987). Following the approach of Vaidyanathan and Tien (1991), we can show that, for streamline flow around the support, the relationship between the expected value of the probability of binding (adhesion efficiency) and the critical angular position, θ_C, on the support past which binding will not occur is

$$P_i = \sin^2(\theta_{c,i}). \tag{4}$$

Substituting the expression for shear rate as a function of angular position given by Tien (1989) into Eq. (4), the adhesion efficiency becomes

$$P_i = \left(\frac{SR_{c,i}d}{3\nu_l A_H}\right)^2, \tag{5}$$

where SR_c is the critical shear rate and A_H is Happel's parameter.

In this expression SR_c is the critical shear rate where the adhesion efficiency is 1. The actual critical shear rate for a given cell–ligand system is a function of several variables (concentration of receptors and ligands, receptor–ligand affinity, receptor mobility, bond formation rate, and contact area) and can be calculated using the adhesion model of Hammer and Lauffenberger (1987). An excellent review by Lauffenberger and Linderman (1993) of this model and other models of receptor–ligand binding is available. The critical shear rate can also be calculated for binding solely on the basis of non-specific forces (electrostatic, London van der Waals, steric stabilization, hydration) using the model of Vaidyanathan (1986). Unfortunately, both of these models contain parameters that are not always available or are difficult to measure experimentally. The adhesion probability is then fit from single population breakthrough curves (Hammer et al., 1987) or measured directly under well-defined conditions using flow chambers (Wattenberger et al., 1990). Once the adhesion probability is determined from a single condition Eq. (5) can be used to estimate the adhesion probability at other experimental conditions.

After combining the equations with the appropriate initial and boundary conditions, the complete set of model equations is determined (Putnam and Burns, 1997). Before the resulting equations are solved, they are dedimensionalized with the following variables:

$$\phi_i = \frac{c_i}{c_{0,i}}, \tag{6}$$

$$\xi = \frac{z}{L}, \tag{7}$$

$$\Theta = \frac{t}{\tau_l}, \tag{8}$$

where ϕ_i is the dimensionless cell concentration (relative to the feed concentration c_0), ξ is the dimensionless axial distance relative to the bed length L, and Θ is the dimensionless time (processing time relative to the residence time of the liquid in the column, $\tau_l = L\varepsilon/v_l$). The result is the following dimensionless equations:

$$\frac{\partial \phi_i}{\partial \Theta} = -\frac{\partial \phi_i}{\partial \xi} - P_i \mathrm{Da}_{I,i}\phi_i\left(1 - \sum_i \psi_i\right)^{\beta_1}, \tag{9}$$

$$\frac{\partial \psi_i}{\partial \Theta} = P_i \frac{\mathrm{Da}_{I,i}}{\kappa_i}\phi_i\left(1 - \sum_i \psi_i\right)^{\beta_i}. \tag{10}$$

The dedimensionalized initial and boundary conditions are the same as those given earlier (Putnam and Burns, 1997).

In addition to P and β for each cell population, inspection of Eqs. (9) and (10) reveal two parameters that govern the performance of the system: a mass capacity ratio, κ, and a first Damköhler number, Da_I, for each population:

$$\mathrm{Da}_{I,i} = \frac{3}{2}(1-\varepsilon)^{1/3}\frac{\eta_{0,i}}{d}L = \frac{\text{Rate of adsorption}}{\text{Rate of liquid convection}}, \tag{11}$$

$$\kappa_i = \frac{\sigma_{m,i}}{c_{0,i}\varepsilon} = \frac{6s(1-\varepsilon)}{c_{0,i}\pi a_i^2 d\varepsilon} = \frac{\text{Maximum number of cells bound (monolayer) on solids in the column}}{\text{Maximum number of cells in one liquid void volume}} \tag{12}$$

From the solution of the model equations using a standard finite-difference technique (Davis, 1984), the purity of the collected effluent and target cell population can be calculated as a function of time. Written in terms of a target cell type (denoted 1) and contaminating cell type (denoted 2), the purities of the target cell population bound and con-

taminating cell type in the *total* collected effluent as a function of dimensionless time are calculated from

$$\psi(\Theta) = \frac{1}{1 + x_2/(x_1 S_b)} = \frac{\text{Number of target cells bound}}{\text{Total number of cells bound}} \tag{13}$$

and

$$\Phi(\Theta) = \frac{1}{1 + \left\{x_1\left(\frac{1}{f_{r,1}} - 1\right)\right\} \Big/ \left\{x_2\left(\frac{1}{f_{r,1}} - \frac{1}{S_r}\right)\right\}} = \frac{\text{Contaminating cell in effluent}}{\text{Total cells collected in effluent}}, \tag{14}$$

respectively, where x is the fraction of ech cell type in the incoming cell suspension. S is the selectivity of the bed in terms of the fraction of each cell type bound,

$$S_b(\Theta) = \frac{f_{b,1}}{f_{b,2}} = \frac{\frac{\kappa_1}{\Theta}\int_0^1 \psi_1 d\xi}{\frac{\kappa_2}{\Theta}\int_0^1 \psi_2 d\xi} = \frac{\text{Fraction of target cell bound}}{\text{Fraction of contaminating cells bound}}, \tag{15}$$

or retained (bound and in the bed void volume),

$$S_r(\Theta) = \frac{f_{r,1}}{f_{r,2}} = \frac{1 - \frac{1}{\Theta}\int_0^\Theta \phi_1 d\Theta}{1 - \frac{1}{\Theta}\int_0^\Theta \phi_2 d\Theta} = \frac{\text{Fraction of target cells retained}}{\text{Fraction of contaminating cells retained}}. \tag{16}$$

Note that at long times the amount of cells in the void volume becomes negligible to the number of cells bound and the selectivity (retained) approaches the selectivity (bound).

MATERIALS

Mined magnetite (Fe_3O_4) was donated by NL Industries (Tahawus, NY). Distilled water was obtained from a Barnstead (Boston, MA) glass still and deionized using a Barnstead Nanopure II deionizer. The lectins *Griffonia simplicifolia* I (GSI) and *Helix pomatia* agglutinin (HpA) were obtained from EY Labs (San Mateo, CA) and Sigma Chemical Co. (St. Louis, MO), respectively. Fluorescamine, *N*-acetyl-D-galactosamine, α-D-methyl-mannopyranoside, and α-D-methylgalactopyranoside were also obtained from Sigma Chemical Co. Polymeric isocyanate (PAPI 901) was generously donated by Dow Chemical (Midland, MI). BB Fluoresbrite™ carboxylate microspheres (365/468 nm, excitation/emission max.) were obtained from Polysciences, Inc. (Warrington, PA). The reported size distributions of the fluorescent microspheres used were 5.0 ± 0.1 and 5.6 ± 0.5 μm. All other chemicals were reagent grade and obtained from commercial sources.

METHODS

Cell Preparation

Adenine-saline (AS-1) added red blood cells (erythrocytes), types A, B, and O, were obtained from the University of Michigan Hospitals Blood Blank (Ann Arbor, MI), centrifuged (7 min, 650*g*), and washed three times using phosphate-buffered saline (PBS, pH 7.4; composition: 0.15 *M* NaCl, 0.1 *M* KCl, 0.01 *M* Na_2HPO_4, Ca^{+2} and Mg^{+2} free); 2–3 mL of erythrocytes processed in this way provided approximately 10^{11} cells.

For analysis of the cell populations, the target cell population was fluorescently tagged with fluorescamine; 100 μL of fluorescamine at 20 mg/mL in acetone was added to each mL of the washed and sedimented erythrocyte suspension. The tagged suspension was then centrifuged (7 min, 650*g*) and washed three times with PBS.

Cleaning of Magnetite Support

Sieving of the magnetite was accomplished using a RX-24 shaker from W. S. Tyler (St. Catharines, Ontario), and this gave the following approximate final size distribution (in μm): >425 (53%), 425–300 (20%), 300–212 (10%), 212–150 (7%), 150–-75 (7%), <75 (3%). Sieved magnetite, 30 g, was then placed in a 200-mL container and shaken vigorously with 150 mL of tap water. Washing was continued until the decanted solution was relatively clear, typically 10 times; 30 g was then placed in the bottom and top trays of a Model 1210R Branson sonicator (Danbury, CT) containing 0.225 *M* NaOH in distilled and deionized water and sonicated for 30 min. Each 30-g sample was then removed from the sonicator and washed by shaking with 150 mL of 0.225 *M* NaOH. This sonication/wash procedure was then repeated two more times. The cleaned support was then washed by placing the support in a 200-mL container and shaking with 150 mL of distilled and deionized water. This was continued until the pH of the decanted solution was near the pH of the distilled and deionized water. After drying overnight at 110°C, the support was then ready for lectin immobilization. The mean diameter of each sieved and cleaned fraction was calculated using the method described earlier (Putnam and Burns, 1997).

Lectin Coupling to Magnetite

The lectins *G. simplicifolia* I (GSI) or *H. pomatia* agglutinin (HpA) were immobilized on the magnetite surface by adapting a process previously developed by Messing and Yaverbaum (1978) to immobilize enzymes on porous metallic (silica and titanium) oxides. Ten grams of magnetite and 12 mL of a 50% solution of acetone and polymeric isocyanate,

PAPI 901, were added to a 15-mL Corning centrifuge tube. The centrifuge tubes were rotated horizontally for 45 min on a Fisher Scientific Hematology/Chemistry mixer (Pittsburgh, PA). The magnetite was then washed in the centrifuge tube four times with acetone and then four times with 0.2 *M* Na_2HPO_4. Ten mL of a 1 mg/mL lectin solution in 0.2 *M* Na_2HPO_4, pH 8.0, was then added to each centrifuge tube. The centrifuge tubes were then rotated horizontally for 2 h where, under the slightly alkaline conditions, unreacted isocyanate groups react with primary amines on the lectin to form a very stable substituted urea. The coupled magnetite was then rinsed four times with 0.1 *M* Na_2HPO_4, pH 7.4, and stored at 4°C.

Cell Binding Assay

Erythrocyte type specific adhesion was assayed in the presence a competing sugar (α-D-methylgalactopyranoside or *N*-acetyl-D-galactosamine for GSI or HpA, respectively) for the lectin binding site. The coupled magnetite was immobilized to a microscope slide that was covered with a thin layer of Dow Corning clear silicone adhesive. To detect bound cells, the cells were pre-tagged with fluorescamine as described in Cell Preparation. One mL of the tagged cell suspension was then added to 2 mL of PBS containing the appropriate sugar at a concentration of 0.2 *M*. A small drop of the tagged suspension was then allowed to sediment onto the surface of the affinity support for 3 min. The slides were gently rinsed with PBS, and the number of bound cells was observed under epifluorescence microscopy (see in situ studies below for a description of the microscope system).

Column Construction

The experimental apparatus, shown in Fig. 1, consisted of a 1-cm i.d. column custom made from 7740 Pyrex glass. Fused into the bottom of each column was a 0.64-cm deep, type B (70–100 μm) sintered glass disk from ACE Glass Inc. (Vineland, NJ) to provide uniform flow distribution while still allowing cells to pass freely. Cell suspensions were pumped (2.9 mL/min) to the column using Masterflex® peristaltic pumps purchased from Cole Parmer Instrument Co. (Niles, IL). The vertically oriented magnetic field was produced by passing DC current through four modified Helmholtz coils (13.5 cm diameter × 2.5 cm thick) spaced 9 cm apart. At a current of 1.6 A (50 W), each coil produced a magnetic field strength of 160 Gauss and required no additional cooling. The bed effluent cell concentration, measured in absorbance units (AU), was monitored with a Perkin–Elmer (Norwalk, CT) Lambda 12 UV/VIS spectrophotometer and UV/WinLab™ software. For absorbance values less than 1, the values were linear with cell concentration.

Column Operation

Unless otherwise stated, the operating conditions are as listed in Table I. The column was filled with PBS (pH 7.4), and the support was loaded with a disposable plastic transfer pipette. The column was gently tapped to allow the support to pack to its minimum void fraction, measured to be 0.42, and the packed bed height was then recorded. To equilibrate the bed with PBS, a Bio-Rad (Hercules, CA) flow adapter column was placed 1 cm above the bed and PBS was passed down through the column until the volume collected was at least five times the bed volume. At this point, if the column was to be operated as a packed bed, the feed to the column was immediately switched to the erythrocyte suspension. For MSFB runs, the flow adapter was temporarily removed and the bed was fluidized with PBS entering below the distributor. With the bed at its expanded height, the flow adapter was again placed 1 cm above the bed and the magnetic field was applied. The feed was then switched to the cell suspension. At the end of the run with the bed still

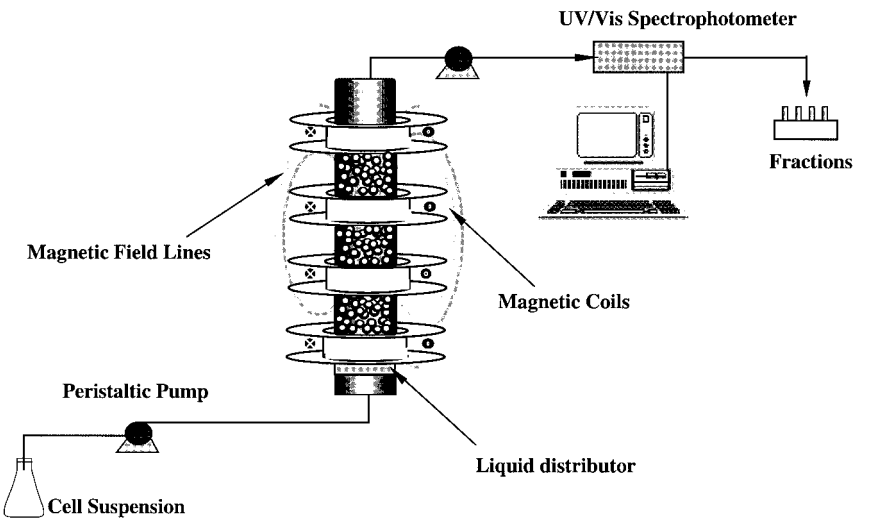

Figure 1. Magnetically stabilized fluidized bed (MSFB) apparatus.

Table I. Standard operating conditions for experiments.

Parameter	Value
Liquid Velocity, v_l	3.7 cm/min
Magnetite support diameter, d	140 ± 32 μm
Erythrocyte Cell Diameter, $2a$	5.6 μm
Column diameter	1 cm
Buffer	Phosphate-buffered saline
pH	7.4

stabilized, the feed was switched to PBS for 15 min to wash unbound cells from the column, and the bound cell fraction could then be recovered.

Analysis of Cell Fractions

The concentration of the labeled cell type was determined by visually counting the number of fluorescent cells in a haemacytometer (Reichert, Buffalo, NY) chamber using a Zeiss Axioskop microscope (Carl Zeiss Inc., Thornwood, NY). The scope was equipped with a 365/500 nm Zeiss excitation/long-pass emission filter set and a Zeiss 20X Epiplan-Neofluar/Brightfield/Darkfield objective (N.A. 0.30) and a 10× projection lens, giving a total magnification of 200×. The total cell concentration was determined by counting all cells, and the non-fluorescent cell concentration was found by subtraction. The concentration of non-intact cells due to cell lysis was correlated with the subsequent release of hemoglobin into solution. Cell lysis led to an increase in the solution absorbance at 414 nm that was proportional to the concentration of non-intact cells.

In Situ Adsorption Studies

An MSFB, used for in situ adsorption studies, was formed in a flow chamber. The chamber consisted of a Plexiglas base (10.2 × 7.62 × 2.22 cm) with feed and exit ports (1.59 mm i.d.), a thin rubber gasket, a standard microscope slide (75 × 25 mm), and an aluminum cover plate (10.2 × 7.62 × 0.95 cm). The Plexiglas base also contained a removable liquid distributor cut from a porous polypropylene sheet (×4903, medium) donated by Porex Technologies (Fairburn, GA). The rubber gasket (0.80 mm thick) had a rectangular notch in it, 70 mm long by 18.6 mm wide, that set the allowable dimensions of the bed. The aluminum cover plate was machined to allow the microscope slide to fit flush into the bottom of the plate and to allow room for movement of the microscope objective. The chamber, after being loaded with support and equilibrated as described for column operation, was placed through two rectangular magnetic coils attached to the stage of a horizontally oriented Zeiss Axioskop microscope (see Fig. 2). The magnetic coils (7.94 × 2.22 cm) were 2.22 cm thick with centers spaced 6 cm apart and consisted of 3.8 m of 24 A.W.G. wire. A 160-Gauss magnetic field was produced by passing 1.5 A through the coils using a Hewlett Packard 6284A DC power supply.

Adsorption of cells was observed under epifluorescence microscopy with a Zeiss Axioskop microscope that was equipped with a 365/500 nm Zeiss excitation/long-pass emission filter set, a Zeiss 10× Epiplan-Neofluar/Brightfield/Darkfield objective (N.A. 0.30), and a 10× projection lens, giving a total magnification of 100×. The image analysis system consists of an Oncor Imaging (Gathersburg, MD) Personal Workstation Real Time Video Frame Grabber/ALU Module, Imaging software (version 1.6), a Hamamatsu Newvicon camera with C2400 controller, and a video cassette recorder. Previously recorded images on a Sony video cassette recorder were played back through a Macintosh IIfx computer and analyzed via Oncor hardware and software. Calibration with a 1-mm square in a haemacytometer showed that at 100× magnification each pixel represented 2.00 × 2.00 μm.

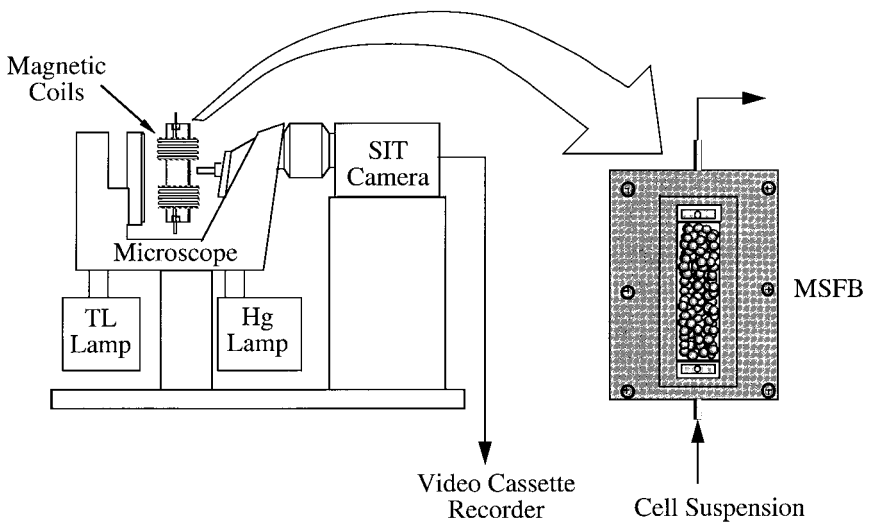

Figure 2. MSFB and microscope system used for in situ adsorption studies.

RESULTS AND DISCUSSION

Erythrocyte Subpopulation Fractionation and Elution

We have used an MSFB to separate erythrocyte populations based on their differing membrane bound sugars. The bed contained magnetite ($d = 140 \pm 32$ μm, $\rho = 4.6 \pm 0.1$ g/mL) to which the lectin *H. pomatia* agglutinin (HpA) had been immobilized. This lectin selectively binds *N*-acetyl-D-galactosamine (D-GalNAc) moieties present on the surface of type A erythrocytes. Using this system we expect that, as a suspension of A and O erythrocytes is passed through the column, a greater fraction of A erythrocytes would bind to the support.

The purity of type O erythrocytes, either adsorbed on the bed or collected from the column effluent, is shown in Fig. 3. The nearly 100% retention of A erythrocytes produces a high, constant effluent purity of O erythrocytes. At the end of the run, the final purity of the collected effluent (~350 mL in 2 h) was 99.7% ± 0.4% with an O erythrocyte recovery of 95% ± 7%. This represents an average 3.1 ± 0.6 log or approximately 1,200-fold decrease in the number of A erythrocytes present in the initial sample. This degree of retention is similar to the 3–4 log required of many clinical cell separation systems (Kemshead and Gee, 1995). Note that the "±" uncertainties represent one standard deviation and the error bars in the figures represent a 90% confidence interval.

The purity of A erythrocytes in the adsorbed fraction was also high. As can be seen from Fig. 3, the purity of retained O erythrocytes, estimated from the fraction of each cell population retained, decreases with time due to the bed's higher capacity for A erythrocytes. At the end of the run, the retained A erythrocyte purity is calculated to be 94%, a substantial increase in purity from its initial value, 50% ± 1%.

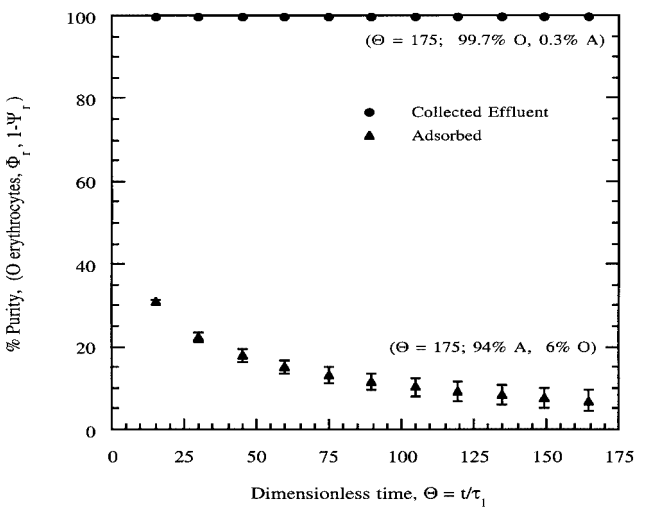

Figure 3. Separation of A and O erythrocytes with *H. pomatia* agglutinin (HpA). The near-complete removal of A erythrocytes results in a high purity of O erythrocytes in the collected effluent. Total number of cells processed is 1.1×10^9. Adsorbed A (O) cell purities were calculated from the effluent concentration profiles for each cell population. The data is an average of six MSFB runs.

Our initial experiments to recover this purified fraction by competitive elution resulted in less than a 1% recovery of bound A erythrocytes. The low recovery of bound A erythrocytes using this method was probably caused by a high surface concentration of HpA. The elution concentration of D-GalNAc in this study (30 mg/mL) is 15 times higher than what we found necessary to recover >90% of bound A erythrocytes from a commercial support, HpA-Sepharose 6MB, available from Pharmacia Biotech (Putnam et al., 1999). In addition to a higher amount of HpA used in the coupling step for magnetite (10 mg per 3 mL of sedimented support versus 3.6 mg per mL of sedimented Sepharose 6MB), the nonporous nature of magnetite compared to porous Sepharose likely led to a significantly higher HpA surface concentration. Hertz et al. (1985) estimated that only a small percentage of coupled ligand on Sepharose 6MB is accessible for binding.

A simple mechanical elution method was then explored. After unbound cells were washed from the column, the field was turned off and the side of the column was gently tapped. Tapping of the column was necessary to induce bed mixing and subsequent cell desorption since even at high fluidization velocities, the magnetite showed little large-scale mixing. Analysis of the recovered fraction showed that, although this method resulted in the detachment of >90% of the cells bound on the column, only 1% of A erythrocytes released were intact. The low concentration of intact A erythrocytes was most likely due to the strong binding of the cells to HpA since the recovery of non-specifically bound O erythrocytes showed no detectable degree of cell lysis.

The most effective elution method was a combination of the two methods: mechanical elution in the presence of a competing sugar for the lectin erythrocyte binding site. At a concentration of 30 mg/mL D-GalNAc, the percentage of eluted A erythrocytes that were intact increased from <1 to 45% ± 6% percent with a resulting increase in purity from 2% ± 2% to 76% ± 5%. This increase in the recovery of intact A erythrocytes upon elution is due specifically to the presence of D-GalNAc since control experiments using a similar non-competing sugar, α-D-methylmannopyranoside, showed no increase. Note that recovery of intact O erythrocytes from both fractions was greater than 90% ± 7%, demonstrating that passage through the bed or mechanical elution is not harmful to the viability of these cells.

Further optimization of the HpA surface concentration would most likely lead to a support with a high capture efficiency but that would release a high fraction of intact cells in the presence of the competing sugar. The HpA surface concentration should be decreased to make elution conditions more gentle. Probably the most effect way to decrease the strength of binding on HpA would be to functionalize the support with a mixture of HpA and a non-cell-binding protein such as human serum albumin. The total protein concentration should be kept the same to minimize non-specific cell binding.

Although elution of the adsorbed fraction proved difficult

due to strong binding of HpA, the experimental results presented demonstrate the feasibility and high selectivity of this system. Additionally, the HpA support facilitated the processing of approximately 1.1×10^9 cells in 2 h. The support was used four times without significant loss of activity. The processing rate of even this unoptimized system is comparable to packed bed CAC systems (Putnam et al., 1999).

Model Verification

In this section we test the ability of the model to characterize the observed adsorption behavior and to provide meaningful values of parameters that govern the interaction of the cells and support. The results of in situ adsorption studies are also presented that provide additional insight into the adsorption behavior occurring in the system. A summary of experimental conditions and model paramters calculated and fitted is shown in Table II.

We first tested the model's ability to describe the binding behavior of single cell populations. Using parameters obtained from independent analysis of the experimental data (see Appendix), the model equations were solved to predict the adsorption behavior of each erythrocyte population. The validity of the parameters obtained using this approach is demonstrated in Fig. 4, where we have plotted the experimental data and model fit for the binding of B and O erythrocytes on magnetite coupled with the lectin *G. simplicifolia* I (GSI). As can be seen from the figure, the model fit to the experimental data is excellent in each case, and the obtained values of the parameters shown in the figure caption confirm the selectivity of the support for B erythrocytes.

Using the model parameters obtained from the single population runs shown in Fig. 4, we next predicted the separation of these populations under the same conditions and compared them with the experimental results. As can be seen from Fig. 5, the model predicts the same trends in the data, predicting a more rapid decrease in the fraction of O erythrocytes retained compared to B erythrocytes and an increase in retained selectivity with time. This trend of increasing selectivity leads to a decrease in the purity of adsorbed O erythrocytes with time as shown in Fig. 6. The predicted purity of the effluent and adsorbed cells at the end of the run (81% O, 19% A; 19% O, 81% A) compares well with the experimental results (91% O, 9% A; 25% O, 75% A).

In addition to describing erythrocyte binding in MSFB systems, we have found that the model is capable of describing the adsorptive behavior in packed bed CAC systems as well. Using parameters determined from a single run in a 0.75-cm bed, the model equations were solved to predict the effect of doubling the packed bed height to 1.5 cm. Figure 7 shows that the model accurately predicts the increased processing capacity of the bed. The effect of bed height is taken into account in the model by Da_I. An increase in bed height not only increases the capacity of the system by increasing the amount of support but also provides an increased residence time for adsorption.

Figure 8 shows a comparison of model predictions using packed bed determined parameters with the experimental results described earlier for the separation of A and O erythrocytes in an MSFB. As can be seen from the figure, despite the higher calculated critical shear rate (see Eq. (5)) for the packed bed (450 s^{-1}) compared to the MSFB (240 s^{-1}), the model predicts quite well the purity of both O erythrocytes in the collected effluent and retained in the bed. These results indicate that, over these shear rates and conditions, the parameters are similar in both CAC systems.

A comparison of the adhesion efficiencies determined for each lectin system shows that the model provides values of this parameter that quantify the selectivity of the support. The value of p for A erythrocyte binding on HpA (3.2) is several times higher than for B erythrocytes on GSI (0.77). This higher adhesion efficiency for A erythrocyte binding is expected as the concentration of HpA reported by the manufacturer to agglutinate a 2% suspension of A erythrocytes (<4 μg/mL) is approximately 5–7 times lower than the value reported for GSI to agglutinate B erythrocytes (~20–30 μg/mL). The fact that the value of P obtained for A erythrocyte binding (see Appendix) was >1 suggests that the expression for η_0 included in Da_I underestimates the fraction of cells that are transported to the surface of the support. Although this effect has been observed earlier for latex adsorption on spherical supports (Putnam and Burns, 1997), the underprediction may also be due to differences in the flow field around the non-spherical magnetite support.

The adhesion efficiency for either ligand–erythrocyte system were not able to be predicted a priori since parameter values necessary to predict the critical shear rate using the theory of Hammarström and Lauffenberger (1987) were unavailable. This happens frequently given that the model parameters are difficult to measure experimentally. However, once the adhesion probability is determined for a single condition, a procedure is outlined below to estimate the adhesion probabilities at other experimental conditions. A high adhesion efficiency for type A erythrocyte binding is not unexpected given that this lectin has six identical carbohydrate binding sites (Hammarström, 1973) and can rapidly agglutinate A erythrocytes at low concentrations.

Prediction of Cell Removal Rate

To predict the removal of cells for new run conditions, the following methods can be used. First, conditions are found, where the experimentally determined adhesion efficiency (see Appendix) is independent of increased shear rate. This occurs under conditions where the shear rate across the support surface is below the critical shear rate and the adhesion efficiency has a value of one. Since P has a value of one the experimental Damköhler number from a single experiment (Da_I^*) is determined and compared with the predicted value of Da_I. The ratio of these values, X, is then used to adjust the theoretically predicted values of Da_I. The Damköhler number for the new conditions $Da_{I,new}$ is calculated and the predicted Damköhler number is then given by $Da_{I,new}^* = XDa_{I,new}$). With a more accurate expression for

Table II. Experimental conditions and model parameter values.

	Fig. 4		Figs. 5 and 6		Fig. 7		Fig. 8	
	Single population	Single population			Single population	Single population		
	Type B erythrocytes	Type O erythrocytes	Separation of B and O erythrocytes		Type A erythrocytes	Type A erythrocytes	Separation of A and O erythrocytes	
Experimental conditions	MSFB (160 Gauss field)	MSFB (160 Gauss field)	MSFB (160 Gauss field)	MSFB (160 Gauss field)	PB	PB	MSFB (160 Gauss field)	MSFB (160 Gauss field)
Bed								
Bed height, L (cm)	4.65	4.65	4.65	4.65	0.75	1.5	4.65	4.65
Void fraction, ε	0.53	0.53	0.53	0.53	0.42	0.42	0.53	0.53
Feed cell concentration, C_0 (#/mL)	1.6×10^6	1.6×10^6	1.6×10^6	1.6×10^6	1.6×10^6	1.6×10^6	1.6×10^6	1.6×10^6
Ligand	GSI	GSI	GSI	GSI	HpA	HpA	HpA	HpA
Calculated model parameters								
1st Damkohler number, Da_I	3.76	3.76	3.76	3.76	1.40	2.79	3.76	3.76
Mass capacity ratio, κ*	960	960	960	960	1500	1500	960	960
Shear rate, SR (1/s)	240	240	240	240	440	440	240	240
								Parameters used were fitted from a PB type O single population experiment (conditions matched those in Fig. 7, 1.5-cm column)
Fitted model parameters								
Adhesion efficiency, P	0.77	0.22	Parameters used were those from the Fig. 4 single population runs		3.2	3.2	Parameters used were those from the Fig. 7 single population runs	0.11
Shadowing exponent, β	5.3	19.0			3.2	3.2		25.1

*Assumes $s = 1$.

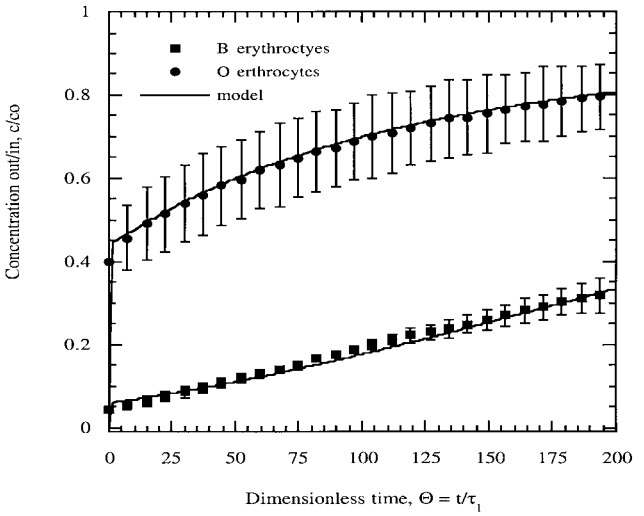

Figure 4. Model fit of B and O erythrocyte breakthrough curves on *G. simplicifolia* I (GSI). The model fits to the experimental data are excellent and provide model parameters for each cell population (B erythrocytes, $P = 0.77$, $\beta = 5.3$; O erythrocytes, $P = 0.22$, $\beta = 19.0$) that quantify the selectivity of the support for B erythrocytes. A higher value of β for type O cells is expected. The shadowing exponent affects the rate of decrease in support binding efficiency as cells bind to the support, and the exponent ultimately determines the capacity of the bed for each cell population. For type B cells this is primarily due to shadowing of other adsorption sites. For type O cells this more just an indication of a very limited number of original sites for non-specific binding. Other model parameters used: $Da_I = 3.76$, $\kappa = 960$. The data for each cell type is an average of two MSFB runs.

the Damköhler number, experiments can now be run to determine experimental adhesion efficiencies. These adhesion efficiencies can be used, in concert with Eq. (5), to determine the experimental critical shear rate (point where the adhesion efficiency starts to decrease) for the cell–ligand system. Eq. (4) can be used to predict the effect of other operating conditions on *P*.

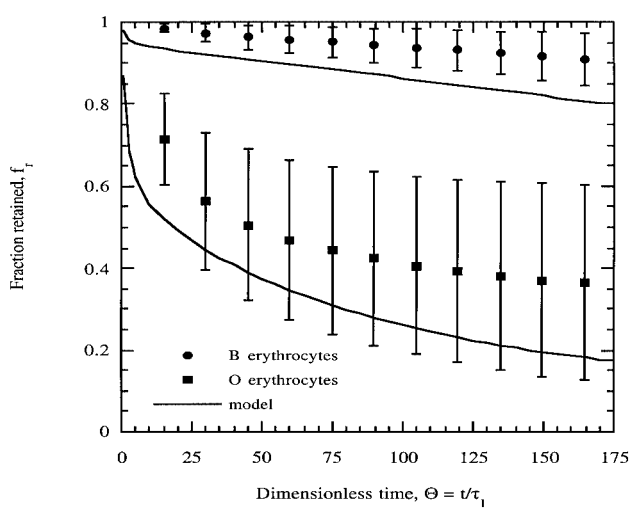

Figure 5. Comparison of model predicted fraction retained data for the separation of B and O erythrocytes on GSI. The model predicts the increasing selectivity of the bed with time. Parameters used were those obtained from the single population runs shown in Fig. 4. The data is an average of three MSFB runs.

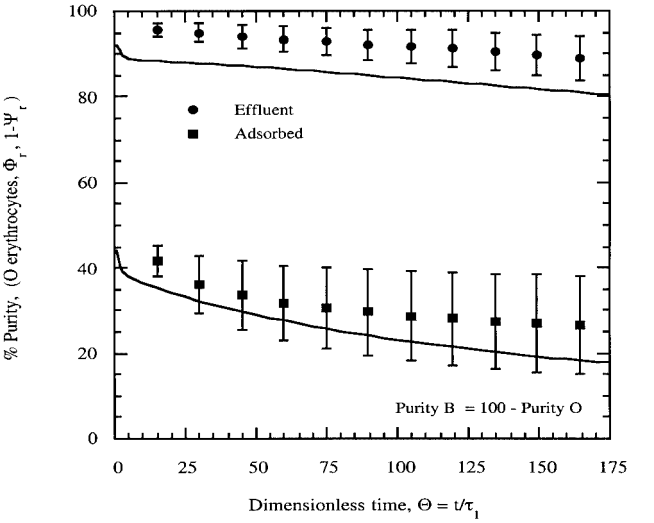

Figure 6. Comparison of model-predicted purities with data for the separation of B and O erythrocytes on GSI. The model predicts quite well the purity of O erythrocytes in the collected effluent and retained in the bed. Parameters were obtained from the single population runs shown in Fig. 4. The data for each condition is an average of three MSFB runs.

Effect of Support Shape

The nonspherical shape of the magnetite particles affected both the predictions of the collection efficiency and the estimation of β. For spherical supports, the trajectories of cells as they approach the support are readily predictable (Tien, 1989). In concert with the critical shear rate for the cell–ligand system, this approach can be used to predict the

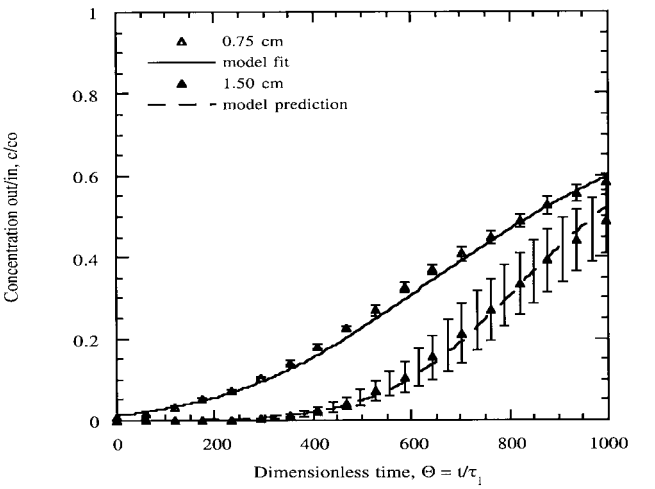

Figure 7. Predicted effect of increased packed bed height on A erythrocyte binding. Using parameters determined from a single set of conditions in a 0.75-cm bed ($PDa_I = 4.46$, $\kappa = 1500$, $\beta = 3.2$) the model accurately predicts the increased processing capacity of the longer 1.5-cm bed ($PDa_I = 8.92$, $\kappa = 1500$, $\beta = 3.2$). The data for each curve is an average of two runs.

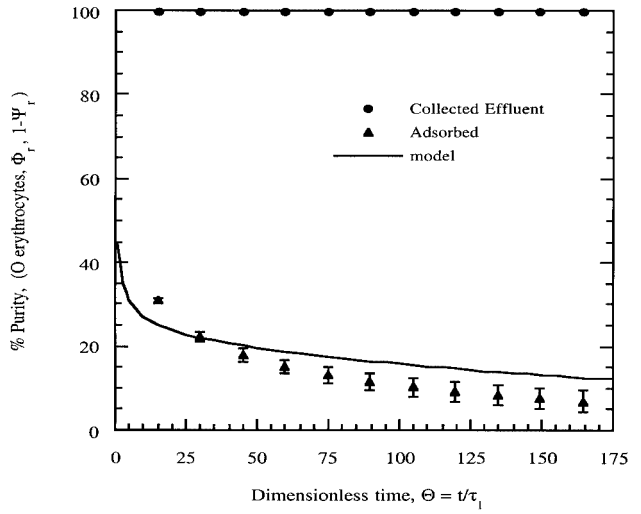

Figure 8. Comparison of model predicted MSFB purities and data for the separation of A and O erythrocytes on HpA. The model predicts O erythrocyte purity quite well using parameters determined from packed bed single population runs. These results indicate that, under these conditions for this cell-ligand system, the parameters are similar in both beds. Parameters used: A erythrocytes, $Da_I = 3.76$, $P = 3.2$, $\kappa = 960$, $\beta = 3.2$; O erythrocytes, $Da_I = 3.76$, $P = 0.11$, $\kappa = 960$, $\beta = 25.1$). The data shown is an average of six runs.

decrease in collection efficiency. However, a trajectory analysis of the magnetite was difficult given the nonspherical shape of the magnetite (see Fig. 9). This non-spherical shape also made it difficult to estimate the surface area available to passing cells. For spherical supports, the area accessible for binding is well defined, since cell trajectories are such that contact with the support can occur only on the bottom half of the support. However, an analysis of the breakthrough curves for A erythrocyte binding on HpA magnetite shown in Fig. 7 revealed that at the end of the run, the fraction of the support surface area that was occupied was calculated to be greater than 50%. Thus, β was calculated from experimental data assuming the entire surface of the support was initially available for binding.

Figure 9. Magnetite support particles (140 ± 32 μm) stabilized in a fluidized bed (darkfield, 100× magnification).

Some of the differences in the adsorption behavior on spherical and non-spherical supports are illustrated in Fig. 10. With similarly sized nickel spheres (Fig. 10a), the flow through the bed was more uniform from below the support, with the adsorption of fluorescent latex spheres (shown in white) occurring primarily on the bottom half the support particles (outlined in gray). However, flow through the bed of magnetite (Fig. 10b) was more tortuous, leading to a direct approach to the flat surfaces of the support and subsequently higher surface coverages in these preferential flow paths (indicated by the arrow) than on the nickel spheres.

These differences in adsorption behavior are accounted for by the low shadowing exponents that we have obtained for magnetite compared to non-specific erythrocyte binding on nickel-based spherical supports under similar conditions. For example, although the adhesion efficiency of B erythrocyte adsorption on an unfunctionalized nickel support (0.81) was similar to the value obtained for B erythrocyte binding on GSI magnetite (0.77), the value of the shadowing exponent was 6.4 times higher for the nickel support. The shape of the magnetite support seems to allow for a more efficient utilization of the support surface area.

Optimizing Cell Separations

While the selectivity of the bed is in large part governed by adhesion efficiencies of each cell type, maximum selectivities can be obtained by choosing experimental conditions that also lead to optimal values of the other dimensionless model parameters. In the previous section, we verified that the model can characterize the experimental results; in this section, we explore the effect of model parameters and experimental conditions on the processing capacity and selectivity of the system.

Processing Capacity

In addition to high purity, a primary goal of the separation is a high retention of the target cell population. As one might expect, the degree of binding is a strong function of the rate of deposition, characterized by Da_I, and the adhesion efficiency, P. Figure 11 shows that these two parameters, which always appear as a product (PDa_I) in the rate expression, strongly affect the retaining capacity of the bed. At low adhesion efficiencies or Damköhler numbers, the bed is adsorption rate limited, leading to early breakthrough, low cell retention, and underutilization of the bed binding capacity. As PDa_I is increased, the degree of cell removal increases, leading to sharp breakthrough curves and maximum processing capacities.

The maximum target cell retention occurs initially during

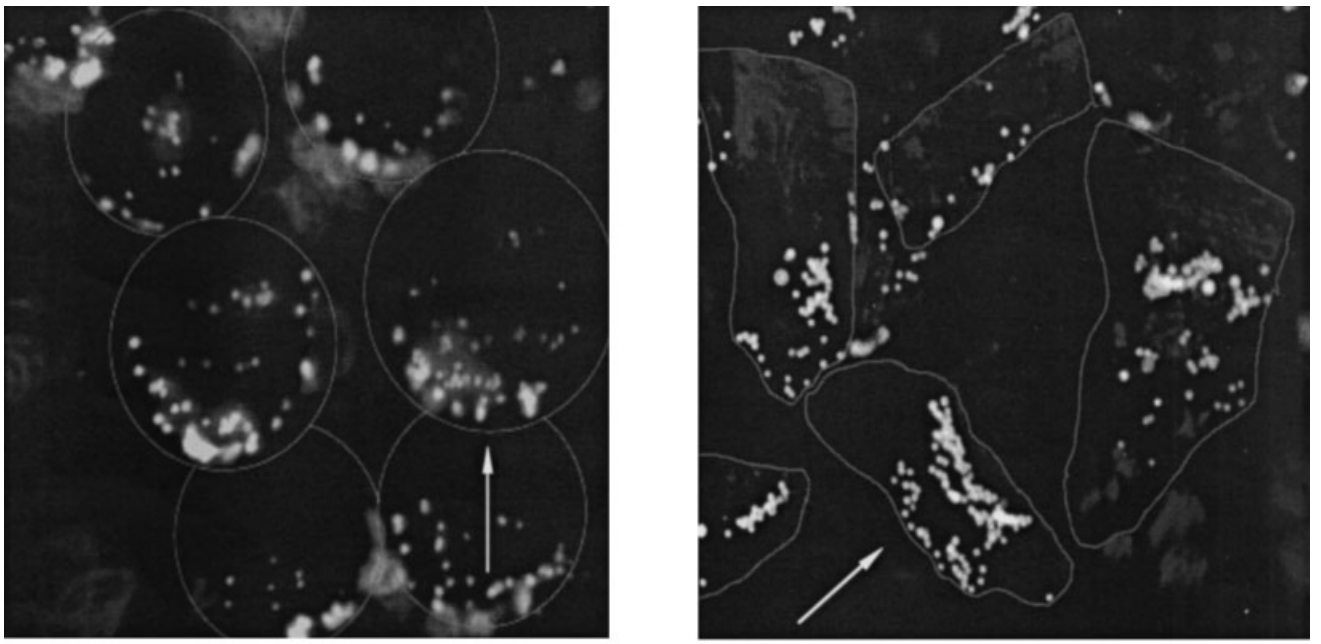

Figure 10. Non-specific adsorption behavior of fluorescent latex spheres. On nickel spheres **(a),** the latex particles (shown in white) adsorb primarily on the bottom half of the spherical support (outlined in gray) while more tortuous flow paths lead to a more direct approach (designated by the arrow) to the flat magnetite support surfaces **(b).** These differences in adsorption behavior seem to suggest a more efficient utilization of the support surface on the nonspherical magnetite. Experimental conditions: **(a)** $2a = 5.0 \pm 0.1$ μm, $d = 140 \pm 32$, $v_l = 34$ cm/min, $\varepsilon = 0.55$; **(b)** $2a = 5.6 \pm 0.6$ μm, $d = 210 \pm 40$, $v_l = 6$ cm/min, $\varepsilon = 0.52$.

the run and is determined solely by $P\mathrm{Da_I}$. For example, Fig. 11 shows that at a $P\mathrm{Da_I}$ value of 2.3, 90% of the cells are retained in the bed, compared to 50% when $P\mathrm{Da_I}$ is 0.69. This relationship between the fraction retained and $P\mathrm{Da_I}$ is given by

$$f_r(\Theta = 1) = 1 - c/c_0(\Theta = 1) = 1 - e^{(-P\mathrm{Da_I})}. \quad (19)$$

This equation is derived from the analytical solution of Putnam and Burns (1997) and predicts the minimum $P\mathrm{Da_I}$ necessary to retain a given fraction of cells. In practice a larger $P\mathrm{Da_I}$ will be required since for processing volumes greater than one void volume ($\Theta > 1$) the fraction retained will decrease with time. The high value of $P\mathrm{Da_I}$ measured for A erythrocyte binding on HpA ($P\mathrm{Da_I} = 12$) is consistent with the near-complete (3.1 ± 0.6 log) retention of A erythrocytes and resulting near 100% purity of O erythrocytes in the collected effluent (see Fig. 8).

In addition to high $P\mathrm{Da_I}$ values, maximum processing capacities occur at high capacity ratios and low shadowing exponents. Figure 12 shows the processing capacity of the bed, defined as the time that the bed can be operated before the exit target cell concentration is greater than 10% of its inlet value, plotted against the effective capacity ratio. This simple plot was adapted from Putnam and Burns (1997) to include P and can be used to estimate to within 15% the number of cells than can be retained (product of the breakthrough time, bed void volume, and inlet target cell concentration). For example, given κ/β values that we obtained for A (300) and O (181) cell binding and a target cell feed concentration of 1.6×10^6/mL, approximately 4.8×10^8 B erythrocytes and 9.4×10^8 A erythrocytes (per mL of bed void volume) can be retained when $P\mathrm{Da_I}$ is 10. Note that the estimated capacity will be affected by the degree of nonspecific binding.

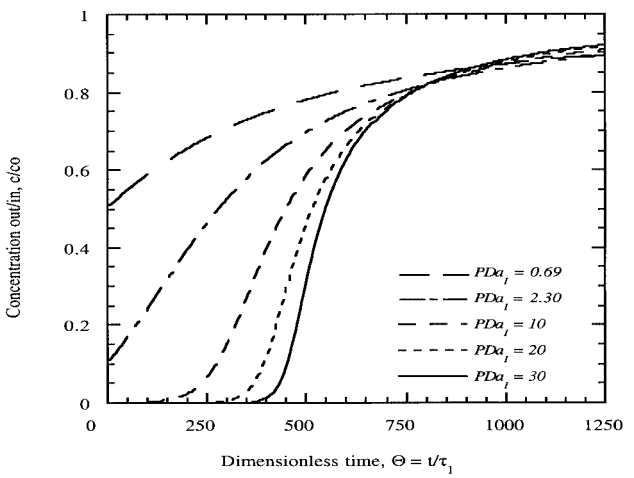

Figure 11. Effect of adhesion efficiency (P) and first Damköhler number ($\mathrm{Da_I}$) on breakthrough behavior. Always appearing together, low adhesion efficiencies or Damköhler numbers lead to adsorption rate limited breakthrough, low cell retention, and underutilization of the bed binding capacity. As $P\mathrm{Da_I}$ is increased, the degree of cell removal increases leading to sharp breakthrough curves and maximum processing capacities. Other model parameters used: $\kappa = 960$, $\beta = 5.3$.

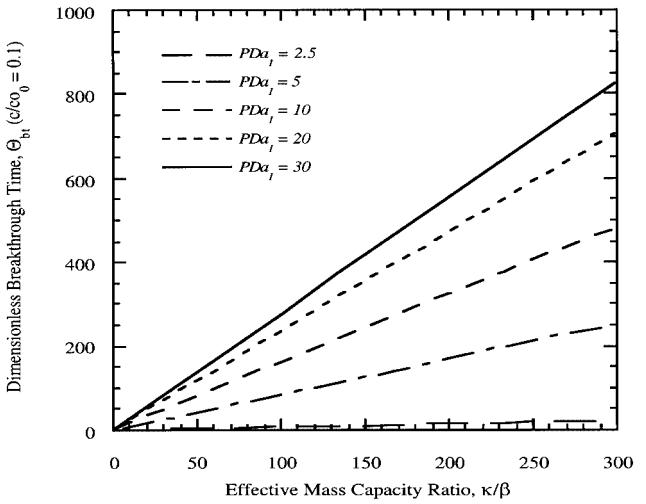

Figure 12. Estimating processing capacities. This simple plot can be used to estimate to within 15% the number of target cells than can be retained (product of the dimensionless breakthrough time, bed void volume, and inlet target cell concentration) before the target cell effluent concentration is greater than 10% of its inlet value.

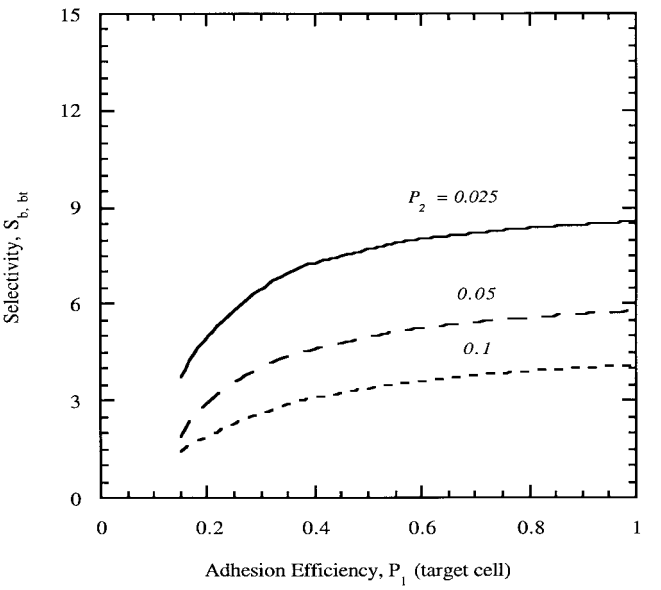

Figure 13. Effect of P_1 on selectivity (defined as $c_1/c_{0,1} = 0.1$). The model predicts that at high P_1 values, decreasing P_2 results in a greater increase in S_b than increasing P_1. Other model parameters used: $\kappa_1 = \kappa_2 = 960$, $Da_{I,1} = Da_{I,2} = 25$, $\beta_1 = 5.3$, $\beta_2 = 19.0$.

Selectivity

The selectivity of the separation arises from the differing capacities of the bed for each cell type. For cases where cell populations are different in size, the larger cells have higher Damköhler numbers, and this has the equivalent effect of an increase in the adhesion efficiency for these cells. Since the majority of the cell populations are very similar or identical in size, the Damköhler number for each cell type is identical, and the selectivity of the bed is primarily due to differences in the adhesion efficiency of each cell population. As Fig. 13 shows, the selectivity, S_b, can be increased by increasing the ratio of the adhesion efficiency of the target cell population (P_1) to contaminating cell population (P_2). As Eq. (5) shows, changes in support diameter, liquid velocity, and void fraction can all affect the adhesion efficiency of each cell type. Other parameters known to affect binding include operating temperature and support ligand concentration (Hammer and Lauffenberger, 1987). Note that, at high P_1 values, a decreasing P_2 results in a greater increase in S_b than increasing P_1.

While the selectivity is affected by the adhesion efficiencies of each cell population, it can also be a strong function of the Damköhler number. For cases where the Damköhler number is identical for each cell type, Fig. 14 shows an optimal Da_I is found to occur in a range where the effective Damköhler number (P_1Da_I) of the target cell population is between 4 and 6. At P_1Da_I values above this range, the high rate of binding toward the front of the bed leaves sites farther down the bed that are accessible to contaminating cell populations and results in decreased selectivity.

The selectivity of the bed is also influenced by the differing shadowing exponents for each cell population. The shadowing exponent affects the rate of decrease in support binding efficiency as cells bind to the support, and the exponent ultimately determines the capacity of the bed for each cell population. As shown in Fig. 15, maximizing selectivity requires decreasing the target cell shadowing exponent (β_1) relative to the shadowing exponent of the contaminating cell population (β_2). Inspection of the β values obtained for erythrocyte binding shows that increased adhesion efficiencies result in decreased β values.

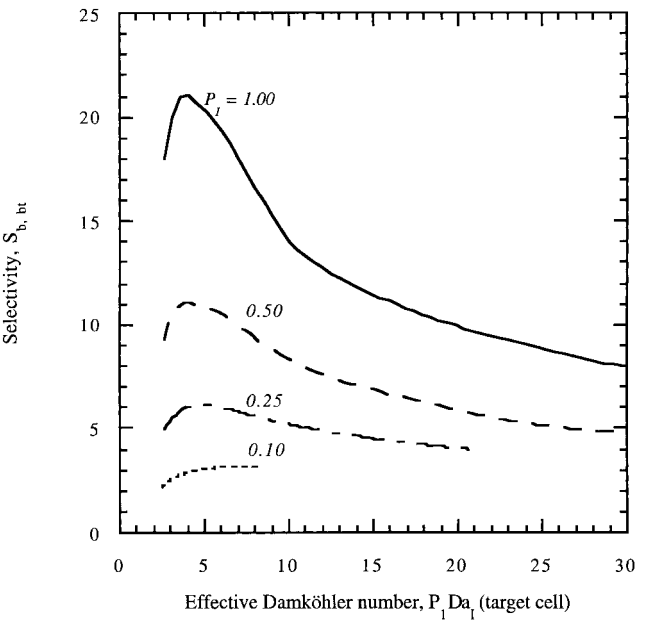

Figure 14. Effect of selectivity (defined at $c_1/c_{0,1} = 0.1$). An optimal Da_I value exists in a range where the effective Damköhler number of the target cell population ($P_1Da_{I,1}$) is between 4 and 6. Other model parameters used: $\kappa_1 = \kappa_2 = 480$, $Da_{I,1} = Da_{I,2}$, $\beta_1 = 2.5$, $\beta_2 = 10$, $P_2 = 0.025$.

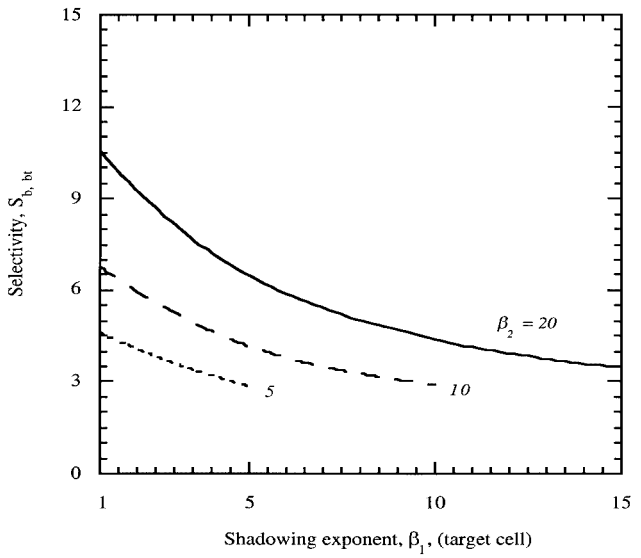

Figure 15. Effect of β_1 on selectivity (defined at $c_1/c_{0,1} = 0.1$). The model predicts that selectivity increases as the ratio of the target to contaminating cell shadowing exponent decreases, and that the rate of increase in $S_{b,bt}$ with β_1 is larger at higher β_2. Other model parameters used: $\kappa_1 = \kappa_2 = 960$, $Da_{I,1} = Da_{I,2} = 20$, $P_1 = 0.8$, $P_2 = 0.05$.

Process Variables

Process variables that can be varied to enhance the processing rate or selectivity of the separation include the processing time, liquid velocity, support diameter, and volume of support material. By far the simplest way to increase the selectivity of the bed is to run the bed for a longer time. Thus far we have calculated selectivity when the target cell concentration exiting the bed is equal to 10% of its inlet feed concentration. However as Fig. 16 shows, using parameters obtained for A and O erythrocyte binding on HpA,

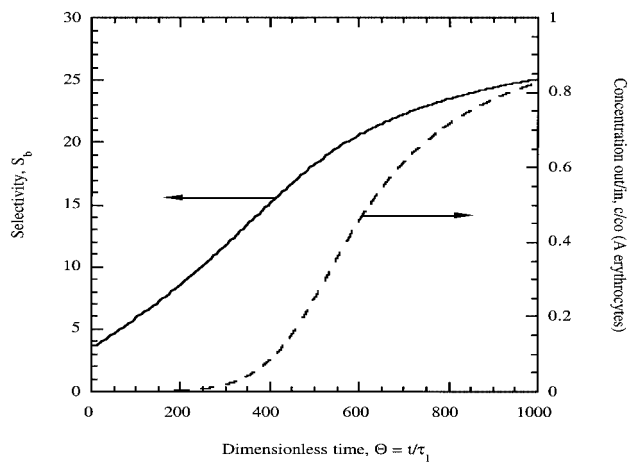

Figure 16. Effect of processing time Θ on selectivity. The simplest way to increase the selectivity of the bed is to run the bed for a longer time. However, the total fraction of target cells retained is decreased. Parameters used were for A and O erythrocyte binding on HpA: A erythrocytes, $Da_I = 3.76$, $P = 3.2$, $\kappa = 960$, $\beta = 3.2$; O erythrocytes, $Da_I = 3.76$, $P = 0.11$, $\kappa = 960$, $\beta = 25.1$.).

the selectivity (bound cells) of the bed is significantly greater at longer times. Of course, the disadvantage of this approach to increasing selectivity is the decrease in the fraction of target cells retained.

The primary advantage of the MSFB system is the ability to gently and rapidly process cell suspensions at high liquid velocities. This increase in throughput of MSFBs at high liquid velocities will require an increase in the amount of support used. As the liquid velocity is increased, the bed void fraction increases giving lower Damköhler numbers, lower capacity ratios and, therefore, lower processing capacities (see Fig. 12). Using a high density support like magnetite minimizes this effect and allows for higher fluidization velocities. The maximum operating liquid velocity will be the one above which the bed can no longer be stabilized.

The low pressure drop characteristics of the MSFB allow the use of long beds that compensate for the decreased deposition rate at high liquid velocities. For example, increasing the liquid velocity above 5 cm/min substantially decreases the Damköhler number. When this effect is coupled with a relatively low adhesion efficiency for B erythrocytes on GSI, the model predicts immediate breakthrough ($c_1/c_{0,1} = 0.1$). However, a 4-fold increase in the amount of GSI support allows the bed to operate at a higher liquid velocity of 11 cm/min. Assuming a negligible decrease in adhesion efficiency at the higher liquid velocity (11 cm/min) and corresponding shear rate, the system can now separate 3×10^9 erythrocytes/h. This processing capacity is an order of magnitude greater than can typically be processed in packed bed CAC systems. Additionally, the predicted number of B erythrocytes retained at breakthrough is 1.45×10^9 ($f_r = 0.96$) with a B erythrocyte purity of 74%. Effluent purity is predicted to be 94% (O erythrocytes).

Changes in the liquid velocity can also be used to increase the selectivity of the system. For example, assuming a negligible change in adhesion efficiencies and shadowing exponents for A and O erythrocytes with increased liquid velocity, increasing the liquid velocity to 11 cm/min from 3.7 cm/min would not only increase the processing rate of an HpA system but also increase the selectivity at breakthrough from 15 to 23. This increase in selectivity is due to an effective Damköhler number (PDa_I) that is closer to the optimal range of 4 to 6. A similar increase in purity can be accomplished through changes in support diameter or changes in both of these process variables.

CONCLUSIONS

We have demonstrated the feasibility of an MSFB for the affinity separation of cell subpopulations. Using various lectins coupled to an affinity support, erythrocyte cell populations were separated on the basis of their differing membrane-bound sugars. Separation of type A and type O erythrocytes with *H. pomatia* agglutinin was very effective, leading to high purities of O erythrocytes in the collected

effluent and A erythrocytes retained in the bed. Strong lectin–erythrocyte binding necessitated using mechanical elution in concert with competitive elution to recover the purified fraction.

In addition to demonstrating the feasibility of the system, a mathematical model was developed and used to determine the running conditions that lead to high selectivities, capacities, and processing rates. At the standard operating conditions, the system provided processing rates that are similar to packed bed systems (10^8/h), while the model predicted that processing capacities at least an order of magnitude greater than packed beds can be easily obtained. This is the first CAC model to account for the decreasing binding efficiency of the support with cell binding and should be useful in analyzing packed bed CAC systems as well.

The authors acknowledge Dr. Irwin J. Goldstein of the Department of Biological Chemistry, University of Michigan, for his valuable discussions and for providing various lectins during the initial studies.

APPENDIX

Calculation of *P* and β from Effluent Concentration Profiles

P and β are obtained from the analysis of the breakthrough curve of a pure cell population. When significant cell breakthrough ($c/c_0 \geq 0.1$) occurs in the first few column void volumes, the cell concentration and support collection efficiency throughout the bed are relatively constant. This allows the following relationship to be derived in terms of the cell concentration exiting the bed (Putnam and Burns, 1997),

$$P\mathrm{Da_I}(1 - \psi^{\beta} = \ln c/c_0 \ (z = L), \qquad \text{(A1)}$$

and the fraction of sites occupied calculated from a simple mass balance on the bed,

$$\psi = \frac{1}{\kappa}\left(\Theta - \int_0^{\Theta} c/c_0 \, d\Theta\right).$$

Experimental values of $P\mathrm{Da_I}$ and β are obtained from a linear plot of $\ln\{-\ln c/c_0 \ (z = L)\}$ versus $\ln(1 - \psi)$, where the slope of the line is β and the *y*-intercept is $\ln(P\mathrm{Da_I})$. $P\mathrm{Da_I}$ is then compared directly to $\mathrm{Da_I}$ calculated from Eq. (11) to calculate *P*.

NOMENCLATURE

Symbols

- a cell radius (μm)
- A_H Happel's parameter [$= 2(1 - \gamma^5)/w$, dimensionless, where $\gamma = (1 - \varepsilon)^{1/3}$ and $w = 2 - 3\gamma + 3\gamma^5 - 2\gamma^6$]
- c number of cells per unit volume of liquid (#/mL)
- d support diameter (μm)
- $\mathrm{Da_I}$ first Damköhler number [$= 3L(1 - \varepsilon)^{1/3} \eta_0/2d$, dimensionless]
- f fraction bound or retained defined by Eq. (15) or (16)
- L bed height (cm);
- P adhesion efficiency (dimensionless)
- R_a rate of adsorption per unit bed volume defined by Eq. (1) (#/mL min)
- s fraction of the support area initially available for binding (dimensionless)
- S selectivity defined by Eq. (15) and (16) (dimensionless)
- SR shear rate (s^{-1})
- t time (min)
- v_l superficial liquid velocity (cm/min)
- x fraction of cell type in feed (dimensionless)
- X ratio of experimental to theoretical Damköhler numbers (dimensionless)
- z axial distance along the bed (cm)

Greek Letters

- σ specific deposit (number of cells per bed volume, #/mL)
- σ_m specific deposit assuming monolayer coverage (#/mL)
- β shadowing exponent (dimensionless)
- ε bed void fraction (dimensionless)
- η collection efficiency (dimensionless)
- η_0 initial collection efficiency (dimensionless)
- φ dimensionless liquid concentration ($= c/c_0$)
- κ mass capacity ratio ($= \sigma_m/c_0\varepsilon$, dimensionless)
- ψ target cell bound purity defined by Eq. (13)
- Φ effluent purity defined by Eq. (14)
- ξ dimensionless axial distance along the bed ($= z/L$)
- ψ fraction of support area occupied by bound cells or particles ($= t/\varepsilon_m$, dimensionless)
- Θ dimensionless time or number of bed void volumes processed ($= t/(L\varepsilon/v_l)$)
- τ_l liquid phase residence time ($= L\varepsilon/v_l$, min)
- θ angular coordinate on the support

Subscripts

- b bound on support
- bt breakthrough, defined when $c/c_0 = 0.1$
- c critical
- r retained in bed (bound and in void volume)
- *i* cell population *i*
- m monolayer
- 0 initial or feed

References

Braun RW, Kümel G. 1986. Separation of T cell subpopulations by monoclonal antibodies and affinity chromatography. Methods Enzymol 121: 737–748.

Burns MA, Graves DJ. 1985. Continuous affinity chromatography using a magnetically stabilized fluidized bed. Biotechnol Prog 1:95–103.

Chase HA. 1994. Purification of Proteins by adsorption chromatography in expanded beds. Trends Biotechnol 12:296–303.

Collins RH Jr. 1994. $CD34^+$ selected cells in clinical transplantation. Stem Cell Transplant 12:577–585.

Davis ME. 1984. Numerical methods and modeling for chemical engineers. New York, Wiley.

de Wynter EA, Coutinho LH, Pei X, Marsh JCW, Hows J, Luft T, Testa NG. 1995. Comparison of purity and enrichment of $CD34^+$ cells from bone marrow, umbilical cord and peripheral blood (primed for apheresis) using five separation systems. Stem Cells 13:524–532.

Fitzgibbons SJ. 1996. Harnessing the immune system. Technol Rev 96: 42–48.

Geankoplis CJ. 1983. Transport processes and unit operations. Englewood Cliffs, NJ: Prentice-Hall.

Greenberg AW, Hammer DA. 2001. Cell separation mediated by differential rolling adhesion. Biotechnol Bioeng 73:111–124.

Hammer DA, Lauffenberger DA. 1987. A dynamical model for receptor-mediated cell adhesion to surfaces. Biophys J 52:475–487.

Hammarstöm S. 1973. Snail (*Helix pomatia*) hemmagglutinin. Methods Enzymol 28:368–382.

Hertz CM, Graves DJ, Lauffenberger DA. 1985. Use of cell affinity chromatography for separation of lymphocyte subpopulations. Biotechnol Bioeng 27:603–612.

Jung Y, Tien C. 1993. Simulation of aerosol deposition in granular media. Aerosol Sci Technol 18:418–440.

Kemshead J, Gee A. 1995. Bone marrow purging. In: Treleaven J, Wiernik P, editors. Color atlas and text of bone marrow transplantation. London: Mosby-Wolfe. p 117–142.

Kernan NA. 1994. T-cell depletion for prevention of graft-versus host disease. In: Forman SJ, editor. Bone marrow transplantation in practice. Edinburgh: Churchill Livingston. p 124–135.

Körbling M, Drach J, Champlin RE, Engel H, Huynh L, Kleine HD, Berenson R, Deisseroth A B, Andreeff M. 1994. Large-scale preparation of highly purified, frozen/thawed $CD34^+$, HLA-DR^- hematopoietic progenitor cells by sequential immunoadsorption (CEPRATE SC) and fluorescence-activated cell sorting: implications for gene transduction and/or transplantation. Bone Marrow Transplant 13:649–654.

Lauffenberger DA, Linderman JJ. 1993. Receptors: models for binding, trafficking, and signaling. Oxford, New York.

Mackie RI, Horner RM W, Jarvis RJ. 1987. Dynamic modeling of deep-bed filtration. AIChE J 33:1761–1775.

Messing RA, Yaverbaum S. 1978. Immobilization of proteins on inorganic support materials. U.S. Patent # 4,071,409, assigned to Corning Glass Works, Corning, NY.

Putnam DD. 1997. Cell separations in fluidized beds: subpopulation fractionation based on affinity adsorption. Ph.D. dissertation. Ann Arbor: University of Michigan.

Putnam DD, Burns MA. 1997. Predicting the filtration of non-coagulating particles in depth filters. Chem Eng Sci 52:93–105.

Putnam DD, Wolf BF, Burns MA. 1999. Cell affinity chromatography. In Kastner M, editor. Protein liquid chromatography. Amsterdam: Elsevier Science.

Reisner Y, Kapoor N, Kirkpatrick D, Pollack MS, Dupont B, Good RA, O'Reilly RJ. 1981. Transplantation for acute leukemia using HLA-A, B nonidentical parental marrow cells fractionated with soybean agglutinin and sheep red blood cells. Lancet 2:327–331.

Riley DJ. 1987. The magnetically stabilized fluidized bed as a solid/liquid separator. M.S. Thesis. University of Massachusetts.

Sharma SK, Mahendroo PP. 1980. Affinity chromatography of cells and cell membranes. J Chromatogr 184:471–499.

Sharon N. 1983. Lectin receptors as lymphocyte surface markers. Adv Immunol 34:213–298.

Sharon N, Lis H. 1989. Lectins. New York: Chapman and Hall.

Terranova BE, Burns MA. 1991. Continuous cell suspension processing using magnetically stabilized fluidized beds. Biotechnol Bioeng 37: 110–120.

Tien C. 1989. Granular filtration of aerosols and hydrosols, Boston: Butterworths.

Vaidyanathan R. 1986. Hydrosol Deposition in Granular Beds. M.S. Thesis. Syracuse: Syracuse University.

Wattenberger MR, Graves DJ, Lauffenberger DA. 1990. Specific adhesion of glycophorin liposomes to a lectin surface in shear flow. Biophysical Journal 57:765–776.